Nanoscale

Accepted Manuscript

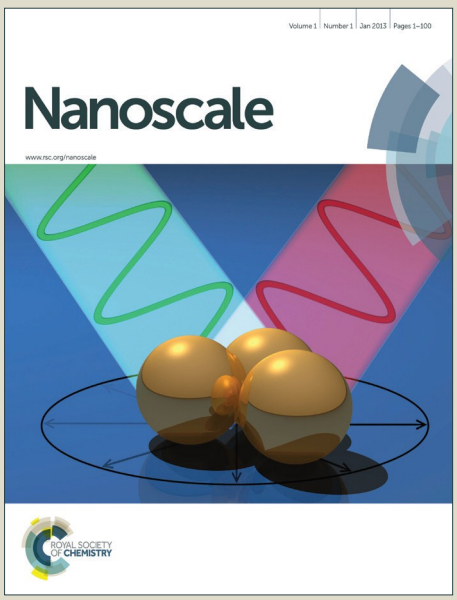

ROYAL SOCIETY OF CHEMISTRY

www.rsc.org/nanoscale

A comparative study of thermo-sensitive hydrogel with water-insoluble paclitaxel in molecule, nanocrystal and microcrystal dispersion

Zhiqiang Lin [a, b], Dong Mei [b], Meiwan Chen [c], Yitao Wang [c], Xianhui Chen [b], Zhaoyang Wang [b], Bing He [b], Hua Zhang [b], Xueqing Wang [b], Wenbing Dai [b*], Yuxin Yin [a*], and Qiang Zhang [b*]

[a] *Institute of Systems Biomedicine, Department of Pathology, School of Basic Medical Sciences, Peking University, Beijing 100191, China*

[b] *State Key Laboratory of Natural and Biomimetic Drugs, School of Pharmaceutical Sciences, Peking University, Beijing 100191, China*

[c] *State Key Laboratory of Quality Research in Chinese Medicine, Institute of Chinese Medical Sciences, University of Macau, Macau 999078, China*

*Corresponding author:

E-mail: pawpaw009@126.com(Dr. W. Dai); yinyuxin@bjmu.edu.cn(Prof. Y. Yin);

zqdodo@bjmu.edu.cn (Prof. Q. Zhang);

Tel/Fax: +86-10-82805724; +86-10-82802791

Abstract

In situ thermo-sensitive hydrogel has attracted increasing attention for alternative cancer therapy due to its long-term and effective drug levels at local site. Besides of synthesizing new thermo-sensitive polymers, we can also fabricate this delivery system by combining hydrogel with thermo-response and drug in different dispersion state, such as drug nanocrystals. However, the impact of drug dispersion state or dimension on the quality of such local injectable system is still unknown. So, here we developed and compared three types of F127 hydrogel systems with paclitaxel or near infra-red probe DiR in molecules (MOs), nanocrystals (NCs) and microcrystals (MCs), respectively. With 120-nm rod-shape nanocrystals, NCs-Gel achieved high drug loading, moderate drug release rate and gel erosion in vitro and in vivo, medium introtumoral drug residue but the best anti-tumor efficacy in 4T1 tumor bearing BALB/c mice. With free drug solubilized in 20-nm micelles of the gel, MOs-Gel system demonstrated the least drug loading and the fast drug release and gel erosion, leading to the least introtumoral residue as well as the lowest anti-tumor effect. Finally, dispersed in micron-grade of rod-shape drug crystals, MCs-Gel exhibited high drug loading but poor precipitating stability in vitro and in vivo, the highest introtumoral residue but the least drug release, resulting in moderate tumor inhibition. In conclusion, this study clarifies the effect of drug dispersion state and scale on the behaviors of a thermo-sensitive hydrogel, indicates the advantage of NCs-Gel system, and provides a basis for the future design of local delivery of hydrophobic anti-cancer agents.

Keywords: Thermo-sensitive hydrogel, Dispersion state, Particle size, Drug loading, Drug release, Anti-tumor efficacy

1. Introduction

Chemotherapy is one of the most important treatments for cancer therapy, but conventional intravenous injection of chemotherapeutic agents only delivers a small percentage of drugs to the tumor site, leading to poor anti-tumor efficacy and severe side effects [1, 2]. Even the nanoparticle-based drug targeting strategy which was widely developed in recent years cannot transport anything better than a few percent of the total dose reaching the disease site [1, 3]. Therefore, localized delivery of chemodrugs provides a good option or alteration for cancer therapy before unprecedented progress in targeting drug delivery system. They could preserve high therapeutic concentrations of drug at the tumor site and reduce systemic distribution of drug, thus enhancing the therapy index of anti-tumor drug [2, 4].

During the last several decades, a variety of localized polymer depot delivery systems have made great progress, including microparticles [5], implantable polymer films [6], expansile nanoparticles [7], polymer milirods [8], *and in situ* thermo-sensitive hydrogel [9]. In these implantable systems, some have been developed successfully and approved by FDA, such as Gliadel Wafer [10]. Especially, unlike other local formulations, *in situ* thermo-sensitive hydrogel is injectable without surgery procedure, attracting more and more attention in recent years. Many thermo-sensitive polymers have been employed in drug delivery, such as PLGA-PEG-PLGA, Pluronic F127 and so on [11,12]. PLGA-PEG-PLGA based OncoGel has entered Phase II clinical trials [11]. Although thermo-sensitive hydrogels possess obvious advantages, there are still some problems need to be addressed. In most cases, they are not satisfactory so far in terms of their drug loading and drug release [13, 14], which are quite vital for the efficacy of a sustained-release system [15]. Low drug loading, rapid or little drug release cannot provide effective drug levels at local site for a long period of time. Similarly, physical instability during the process of storage and release may limit their efficacy as well [16].

To address the problems on drug loading and drug release for localized drug delivery

system, combination strategies with drug particles and thermo-sensitive hydrogel has been proposed by some groups. Drug-loading liposomes [17], nanoparticles [18], polymeric nanocapsules [19] or microspheres [20] instead of free drugs were opted to be incorporated into the hydrogel for the purpose of preventing the drug from precipitates or prolonging drug retention [17]. For example, a thermo-sensitive Pluronic F127-based hydrogel containing PTX-liposomes achieved slower and more homogeneous drug release as well as higher drug loading [17]. But combination strategies did not necessarily lead to a desired anti-tumor effect of hydrogel. According to a report on hyaluronic acid hydrogel with Taxol and PTX particles, gel did not delay the release of PTX from the 14-nm micelles in Taxol due to the small particle size of micelles, while gel did not prevent aggregation and precipitates of microparticulate PTX which was too large in particle size. Neither PTX micelles nor PTX suspensions could provide the hydrogel with steady drug release at local site [16]. Therefore, the characteristics of particles are required to be designed precisely for constructing these combination hydrogel systems.

In our previous studies, we proposed a combination strategy of incorporating PTX nanocrystals (NCs) into the thermo-sensitive hydrogel (Gel) which realized high drug loading, long-term effective drug release as well as good anti-tumor efficacy [21]. However, the impact of drug dispersion state and dimension on the quality of a local injectable thermo-sensitive hydrogel for antitumor therapy is still unknown. In other words, it remains unclear whether the thermo-sensitive hydrogel with drug nanocrystals is the optimal combination in terms of desired drug loading and effective drug release. So far there was no comparison among the hydrogel systems with different drug forms, such as drug molecules (MOs-Gel), drug nanocrystals (NCs-Gel) and microcrystals (MCs-Gel). Theoretically, the quality of such hydrogel systems may be very different when water-insoluble drugs are dispersed in the gels with different states. For instance, MCs-Gel may loaded more drug, remain locally and release drug for longer time, while MOs-Gel may be just the opposite. Therefore, it is necessary to conduct such a comparative study for different types of PTX hydrogels to find out which one is the most suitable for local cancer therapy. This will provide a basis for the

future design of thermo-sensitive hydrogel.

In the present study, we designed and fabricated three types of hydrogels loaded with water-insoluble paclitaxel in molecule, nanocrystal and microcrystal, respectively, in order to identify the impact of drug dispersion state and dimension on the in vitro and in vivo behaviors of a local injectable thermo-sensitive hydrogel for antitumor therapy (Fig. 1). We then conducted a comparative study on their differences in paclitaxel particle size, morphology, drug loading, drug release, gel erosion in vitro and in vivo and introtumoral drug residue, as well as the anti-tumor efficacy in 4T1 tumor bearing BALB/c mice.

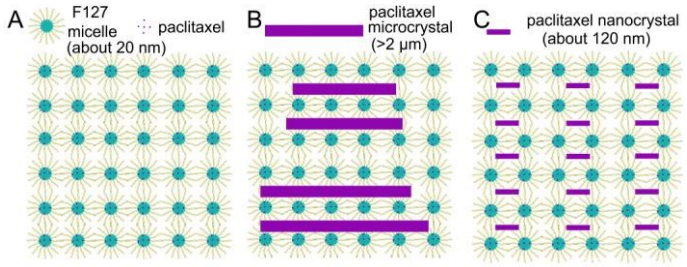

Fig. 1 Diagrammatic sketch of thermo-sensitive F127 hydrogel systems with hydrophobic paclitaxel molecules (A) microcrystals (B) or nanocrystals (C), respectively.

2. Materials and methods

2.1. Materials

Paclitaxel (PTX) was purchased from Haikou Pharmaceutical Co., Ltd. (Hainan, China). Pluronic® F127 (F127, MW=12,600, PEO_{99}-PPO_{67}-PEO_{99}), Tween 80 (Polysorbate 80, MW=1309), sulforhodamine B (SRB) and tris(hydroxymethyl) aminomethane (Tris base) were obtained from Sigma-Aldrich (St. Louis, MO, USA). Fluorescent agent 1,1-dioctadecyltetramethyl indotricarbocyanine iodide (DiR) was supplied from Biotium Inc. (Hayward, CA, USA). All other reagents and solvents were of analytical grade.

RPMI-1640, penicillin/streptomycin and trypsin were the product of M&C Gene

Technology (Beijing, China). Fetal bovine serum (FBS) was purchased from Gibco, Invitrogen Corp. (Carlsbad, CA, USA). Tissue culture flasks were provided by Corning-Costar (Cambridge, MA, USA).

4T1 cells were kindly provided by Professor Wei Liang who purchased it from ATCC [22]. Cells were grown in RPMI-1640 medium supplemented with 10% fetal bovine serum (FBS), and 1% penicillin/streptomycin in a humidified incubator containing 5% CO_2 at 37 ℃.

Female BALB/c mice or ICR mice (18-20 g) were purchased from Peking University Health Science Center (Beijing, China) and kept under SPF conditions for 1 week before the study, with free access to standard food and water. All care and handling of animals are abided by the guidelines of care and use of laboratory animals of the Institutional Animal Care and Use Committee of Peking University.

2.2 Preparation of the three types of hydrogel systems

2.2.1 Preparation of PTX-NCs-Gel and DiR-NCs-Gel

PTX-NCs-Gel was prepared following two steps including the stabilization of nanocrystals and "cold" method for hydrogel preparation [21, 23, and 24]. Briefly, PTX-NCs solution was prepared by solubilizing PTX and F127 (weight ratio = 1:5) in dichloromethane, which then was under a serious of operations such as blowing, vacuum drying, hydration, vortexing and sonication. Under magnetic stirring at 4 ℃, the obtained PTX-NCs solution was added to F127 granules with the final F127 concentration of 20% (w/w). Several hours later, PTX-NCs-Gel formed at the *Sol* state. It was then stored at room temperature (25 ℃) to keep *Gel* state.

For the *in vivo* fluorescence imaging investigation, the near-infrared spectrum fluorescent (NIRF) agent DiR was used to prepared DiR-NCs-Gel following the same protocol as that of PTX/DiR hybrid NCs, which were prepared and confirmed in our previous work [21].

2.2.2 Preparation of PTX-MOs-Gel and DiR-MOs-Gel

PTX-MOs-Gel or DiR-MOs-Gel was prepared using the "cold" method. Briefly, upon magnetic stirring at 4 ℃ for several hours, solution was obtained by mixing appropriate amount of water, F127 and Tween 80 which could prevent the PTX from drug precipitates during the following process [25]. The final concentration of F127 and Tween 80 were fixed at 20% and 12.5% (w/w), respectively. Then, the required amount of PTX ethanol solution or DiR ethanol solution were added into the solution at 4 ℃ and gently mixed for over 6 h.

2.2.3 Preparation of PTX-MCs-Gel

For preparation of PTX-MCs-Gel, blank F127 gel was prepared firstly by mixture 2 g of F127 and 8 ml of deionized water under stirring mixture at ice bath for several hours. Then, 12 mg of PTX power was added into 4 ml of blank F127 gel (20%, w/w). After stirring at 4 ℃ for several hours, PTX-MCs-Gel was prepared.

2.3 In vitro characterization of the three types of hydrogel systems

2.3.1 Particle Size and morphology

To investigate particle size and morphology of PTX dispersed in the hydrogels. Each gel sample was diluted by appropriate fold using deionized water prior to measurement.

Particle size distribution of various samples were determined by dynamic light scattering (DLS) using a Malvern Zetasizer Nano ZS (Malvern, U.K.) at 25 ℃. The morphological shapes of different samples were imaged by transmission electron microscope (TEM, JEM-1230, JEOL, JAPAN) with an acceleration voltage of 80 kv. The 20-fold dilution of PTX-MCs-Gel was further imaged using an inverted microscope due to micron-grade particle

size.

2.3.2 Content of free drug

To determine the percentage of PTX or DiR entrapped in the hydrophobic domains of hydrogels, high performance liquid chromatography (HPLC) or fluorescence spectroscope assay were used to calculate the content of free drug of different formulations. Briefly, each hydrogel was diluted 10-fold using deionized water and then filtrated through a 50 nm polycarbonate filter paper.

Then the filtrate was withdrawn and dissolved by adding 10-fold methanol. After that, PTX was determined with HPLC system with a UV detector (Shimadzu, LC-10AT, Japan). The analysis was performed on ODS column (phenomenex® C18, 5 μm, 250 × 4.6 mm). The mobile phase was a mixture of acetonitrile and water (56:44, v/v). The detection wavelength was set at 227 nm and the flow rate was 1.0 ml/min. DiR was quantified using a fluorescence spectroscope (Cary Eclipse, Varian Corporation, USA). The excitation and emission wavelength were set at 720 nm and 790 nm, respectively.

Finally, the content of free drug was calculated using the following formula.

Content of free drug (%) = PTX concentration in filtrate / total PTX concentration in dilution before filtration ×100%

2.3.3 Storage stability of the three hydrogels

Various PTX hydrogels were placed in three sample vials and stored at room temperature, respectively. At day 0 and day 7, the bottoms of the vials were pictured by a digital camera. Meanwhile, 100 μl of gel on the surface (upper part) or at the bottom (lower part) was withdrawn for quantitative assay. The withdrawn samples were diluted by 10-fold methanol for PTX determination by HPLC. The samples were eluted in an ODS column (Phenomenex® C18, 5 μm, 25 0 × 4.6 mm) in a HPLC system (Shimadzu, LC- 10A T, Japa

n). The mobile phase was a mixture of acetonitrile and water (56:44, v/v) with a flow rate of 1.0 ml/min. The detection wavelength was set to be 227 nm.

2.4 In vitro erosion of the three hydrogels and drug release

In vitro erosion experiments of the three types of PTX hydrogel systems were performed in three 5-ml tubes. 1 ml of hydrogel at 4 ℃ were placed into 5 ml EP tubes and incubated at 37 ℃. Then, 3.8 ml of pre-warmed PBS was carefully layered over the surface of the gel, and the tubes were placed in a thermostatic shaker (100 rpm, 37 ℃). At various time points, the medium was withdrawn and replaced with an equal volume of PBS. The concentration of PTX in the release medium was determined by HPLC-UV under the same conditions as in Section 2.3.3. The cumulative percentage of PTX released was calculated and plotted. At the beginning and the end point of this experiment, each tube was pictured by a digital camera.

In vitro erosion of DiR-MOs-Gel and DiR-NCs-Gel were then performed following the above protocol using DiR as fluorescence probe for molecular imaging. At various time points, the tubes were withdrawn from the shaker and NIRF imaging experiments were performed. NIRF imaging was captured using the Maestro *in vivo* imaging system (CRI, Woburn, MA, USA; λex 720nm, λem 790 nm long pass).

2.5 In vivo erosion of the three hydrogels

To study gel formation and erosion *in vivo*, healthy female mice (20-22 g) were divided into three groups who received subcutaneous injection of 500 μl of PTX-MOs-Gel, PTX-NCs-Gel, PTX-MCs-Gel, respectively. At 0.5 h and 3 d, the mice were sacrificed. The skin was made an incision at the injection sites which were then pictured by a digital camera.

To further investigate the differences between MOs-Gel and NCs-Gel, other healthy female mice (20-22 g) were divided into two groups treated with 100 μl of DiR-MOs-Gel or DiR-NCs-Gel, respectively. The dosing for each mouse was equivalent to 31 μg/kg DiR. The

mice were imaged using an molecular system (CRI, Woburn , MA , USA; λex 720 nm, λem 790 nm long pass).

2.6 *Intratumoral drug residual amount assay and fluorescence distribution*

Armpit breast cancer model was established by inoculating 1.0×10^6 4T1 cells in the right flank of each BALB/c mouse. When tumor volume reached about 500 mm^3, mice were divided into three groups who received a single intratumoral injection of 100 μl of PTX-MOs-Gel, PTX-NCs-Gel, PTX-MCs-Gel, respectively. At day 20 post administration, mice were sacrificed for tumor collection. The residual PTX in tumor mass was qualified by HPLC according to our previous methods [21].

To further observe the fluorescence distribution in tumors, 100 μl of DiR-MOs-Gel or DiR-NCs-Gel was intratumorally injected into the mice, respectively. At day 7 and day 16, the mice were sacrificed and tumors were collected for *ex vivo* imaging. The excised tumors, bisected tumors and sliced (approximately 3 mm sections) were imaged using a molecular system with the same parameters in Section 2.5.

2.7 Anti-tumor activity

The anti-tumor activity was investigated on 4T1 tumor model. 4T1 marine breast cancer models were established as the method in Section 2.6.

When the solid tumor volume reached about 500 mm^3, mice were randomly divided into three groups treated with a single intratumoral injection of PTX-MOs-Gel, PTX-NCs-Gel or PTX-MCs-Gel. The tumor width and length of each mouse was measured every other day using vernier calipers for calculating the estimated size as $[(\text{length}) \times (\text{width})^2/2]$ [26]. At the day 20, the mice were sacrificed by cervical vertebra dislocation. Tumors were then excised and weighted.

2.8 Statistical Analysis.

Quantitative data are shown as means ± standard deviation (SD). Either Student's t test or a one-way analysis of variance (ANOVA) was performed to evaluate the results. A *p*-value less than 0.05 were considered to be statistically significant.

3. Results

3.1. Appearance of the three hydrogels

Fig.2 shows the picture of the three types of freshly prepared hydrogels, which exhibited sol-gel transition properties with temperature changes. Different appearances were observed on the sol samples with various drug dispersion states, transparent for MOs-Gel, nattier blue for NCs-Gel and opacified for MCs-Gel. But the color differentiation between NCs-Gel and MCs-Gel was not obvious at semisolid gel states.

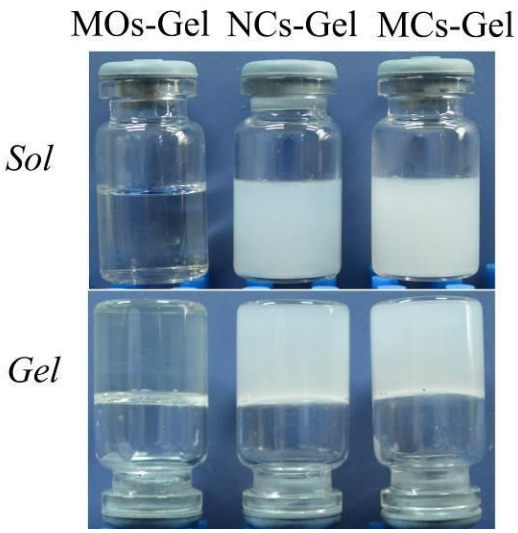

Fig. 2 Appearance of MOs-Gel, NCs-Gel and MCs-Gel which are in *Sol* state at 4℃ or *Gel* state at 37℃.

3.2 Drug dispersion states in the three hydrogel systems

The hydrogel systems were firstly diluted by 20-fold deionized water and then characterized by different means including TEM, microscopy, DLS and HPLC. As shown in Fig. 3, there were different drug states in F127 gel system: NCs, micelles and microcrystals. Specifically, PTX or DiR was dispersed in NCs-Gel in the form of nanocrystals (Fig. 3A and B) while micelles (about 20 nm) or micelle aggregates were observed in MOs-Gel, indicating PTX or DiR was probably solubilized into the hydrophobic domains of the gel (Fig. 3C and D). Fig. 3E and F demonstrate that MCs-Gel contained micron-grade rod-shape PTX crystals longer than 2 μm.

Fig. 4 depicts the differences among the three hydrogel systems in particle size. Based on the DLS analysis, MOs-Gel had a micelle size of about 20 nm after appropriate dilution while MCs-Gel suspended microcrystal with the size of larger than 800 nm. Expectedly, NCs-Gel exhibited a particle size of about 120 nm, intermediating between the former two.

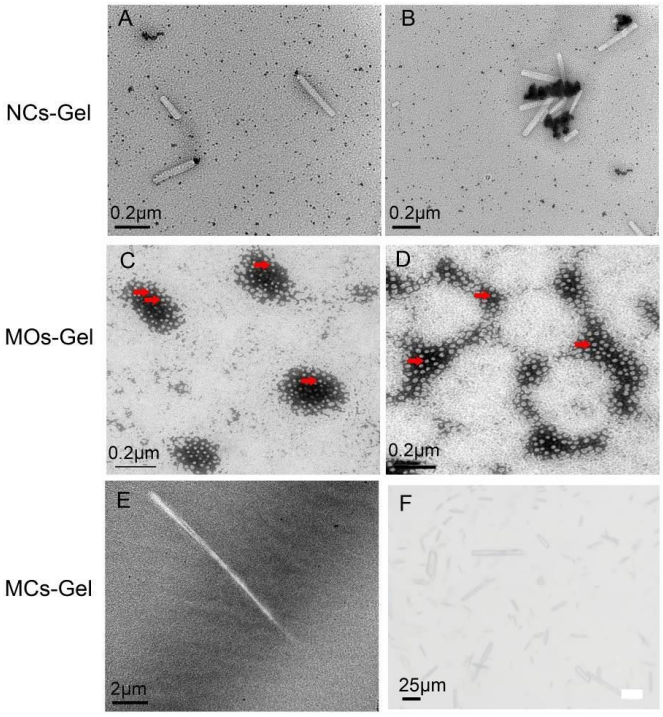

Fig. 3 Transmission electron microscope (A-E) and microscope (F) photos of various F127 thermo-sensitive hydrogel systems upon 20-fold dilution. The samples were PTX-NCs-Gel (A), DiR-NCs-Gel (B), PTX-MOs-Gel (C), DiR-MOs-Gel (D), PTX-MCs-Gel (E, F), respectively. The white dots were F127 micelles indicated by arrows. Bar: 0.2 μm (A-D), 2 μm (E), 25 μm (F).

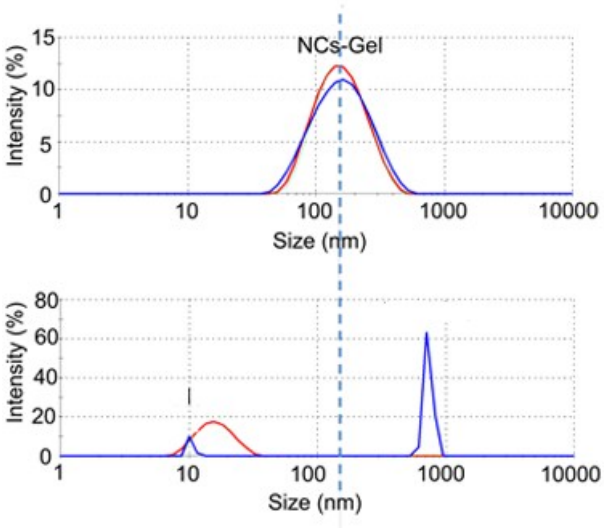

Fig. 4 Particle-size assay of different hydrogel systems. The semisolid gel was subject to appropriate dilution by deionized water before particle size determination by DLS assays. The initial samples include PTX-NCs-Gel (upper panel, blue peak), DiR-NCs-Gel (upper panel, red peak), PTX-MOs-Gel (bottom panel, left blue peak), DiR-MOs-Gel (bottom panel, red peak), PTX-MCs-Gel (bottom panel, right blue peak).

Table.1 lists the main characterizations of various hydrogel systems. Besides of qualitative assay based TEM and DLS, we performed a quantitative assay on their compositions to further confirm whether PTX-MOs, PTX-NCs and PTX-MCs are the dominant drug forms in the corresponding hydrogels. Determination of free drug reflects the partition ratio of paclitaxel in the hydrophobic domains and hydrophobic domains. For NCs-Gel, less than 5% of free drug content suggested that PTX was hardly solubilized into the hydrophobic domains of the hydrogel as molecules. Similarly, MCs-Gel also showed extremely low content of free drug, revealing that PTX mainly suspended in gel instead of being solubilized. In contrast, free drug content in MOs-Gel group was about 100%, illustrating that PTX or DiR were almost completely solubilized into the hydrophobic domains of hydrogel as molecules, consistent with TEM results in which no PTX crystals were observed.

Table. 1 *In vitro* characterization of various hydrogel systems

Categories	Samples	Drug levels	Ingredients (TEM)	Particle Size (DLS)	Content of free drug (%, HPLC)
Nanocrystal-dispersed hydrogel	PTX-NCs-Gel	0.3mg/ml PTX	NCs, Micelles	120 nm	3.07%
	DiR-NCs-Gel	3 mg/ml PTX 6.25 μg/ml DiR	NCs, Micelles	120 nm	3.29%
Molecule-dispersed hydrogel	DiR-MOs-Gel	6.25 μg/ml DiR	Micelles	30 nm	98.3%
	PTX-MOs-Gel	0.3mg/ml PTX	Micelles	30 nm	103.1%
Microcrystal-dispersed hydrogel	PTX-MCs-Gel	3 mg/ml PTX	Microcrystals Micelles	>800nm	4.8%

3.3 Stability of the three hydrogels

Fig. 5A shows physical stability of the three gel systems *in vitro*. After storage in sample vials at room temperature for 1 week, neither PTX-MOs-Gel nor PTX-NCs-Gel exhibited significant visible changes. However, white solid substance precipitated from PTX-MCs-Gel, suggesting its instability.

The stability of the three hydrogel systems was further verified by a quantitative HPLC assay on drug-dispersion uniformity (Fig. 5B). The ratio of PTX levels at upper or lower part of PTX-NCs-Gel and PTX-MOs-Gel were about 50%, maintaining constant during 7 days. However, the percentage of PTX levels at lower part of PTX-MCs-Gel increased significantly from 50% to about 66% under the same storage condition.

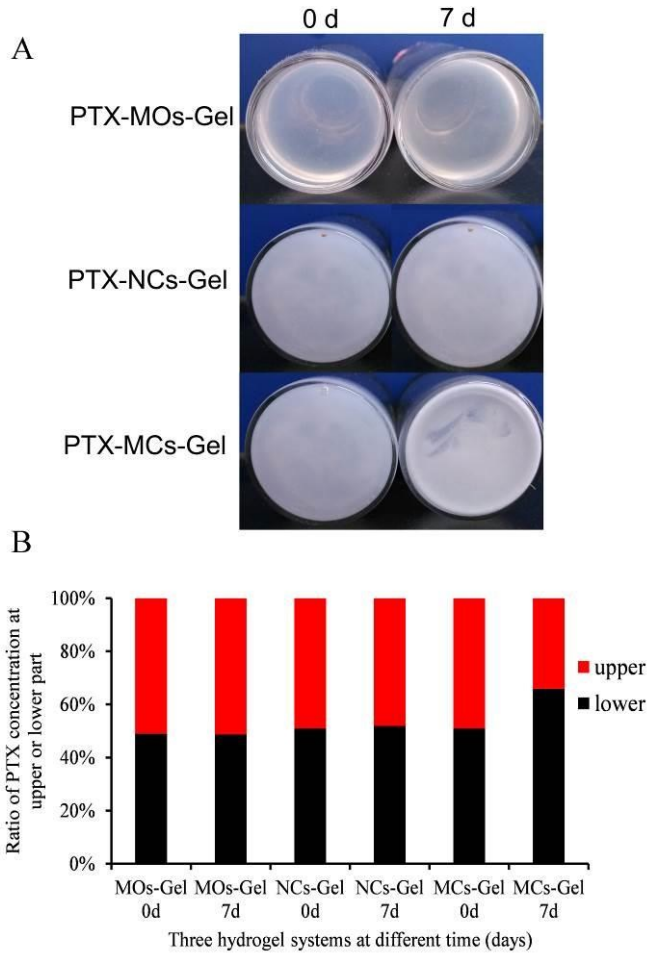

Fig. 5 *In vitro* stability (A) and drug-dispersion uniformity (B) of the three hydrogel systems. After storage at about 15℃ for a week, neither PTX-MOs-Gel nor PTX-NCs-Gel showed significant changes while white solid substance precipitated from PTX-MCs-Gel. These results were also verified by a quantitative assay on drug-dispersion uniformity which suggested the ratio of PTX levels at lower part of PTX-MCs-Gel increased significantly during the storage process.

3.4 In vitro erosion of the three hydrogels and drug release

As shown in Fig. 6A, obvious differences were observed in *in vitro* gel erosion experiments among the three hydrogel systems. At day 0, transparent or white gel formed at the bottom of tubes, and there were phase interfaces between the gel and PBS. The phase interface of MOs-Gel is not as clear as the other two, mainly because of low contrast between gel and PBS. Two weeks later, the phase interface of MOs-Gel disappeared. According to PTX concentration of the samples withdrawn from the medium, almost 90% of PTX had already

been released from the PTX-MOs-Gel (Fig. 6B). Moreover, the particle size in this system was found less than 30 nm which was exactly equivalent to the size of micelles (Data not shown). So, it was clear that during the process of *in vitro* erosion, the drug-loading micelles were released into PBS from the MOs-Gel, making the whole system homogeneous.

Conversely, white solid PTX crystals precipitated apparently from the MCs-Gel system, which released only less than 5% of PTX into medium. Interestingly, NCs-Gel became swelling and loosening upon PBS erosion without any observed PTX precipitates. The cumulative drug released into medium in this gel was also very low, indicating that PTX-NCs-Gel preserved stable drug release.

Because molecules and nanocrystals cannot be visualized by naked eyes, we next performed a similar experiment using DiR as fluorescence probe to further compare the differences of *in vitro* erosion between MOs-Gel and NCs-Gel. As shown in Fig. 6C, this molecular imaging technique could clearly present the dispersion process of fluorescence of DiR from the bottom of tube into the upper PBS. The strong fluorescence in DiR-MOs-Gel group at the bottom of tube dispersed into the medium more quickly than that in DiR-NCs-Gel group. Compared to DiR-MOs-Gel, DiR-NCs-Gel showed more extensive fluorescence at the bottom of tube, especially from day 3 to the end of test, suggesting its stronger local fluorescence retention ability. The heterogeneous fluorescence signals in the upper medium might indicate the hydrogel transportation in PBS medium. So, this study demonstrated the same conclusion as above that the gel erosion and drug release was faster in DiR-MOs-Gel group. Besides, it is worth noting that fluorescence intensity of both systems decreased gradually, or even disappeared totally at last. We believed that it resulted from quenching of DiR caused by long-term exposure at 37 ℃ [27].

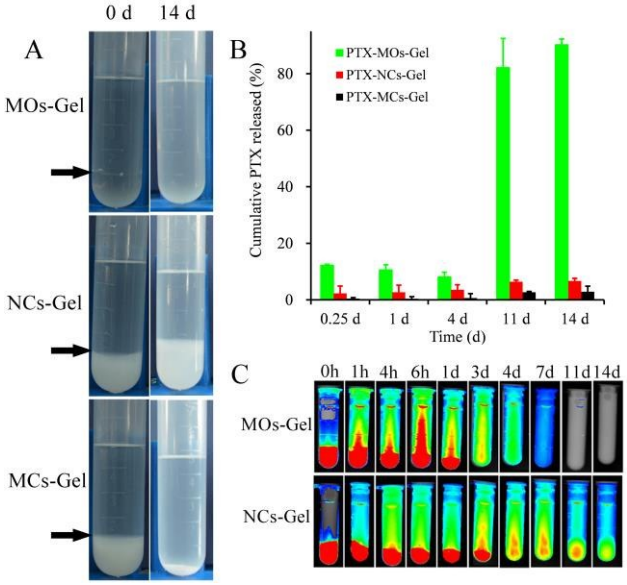

Fig. 6 *In vitro* gel erosion and drug release of three hydrogels in PBS medium. 1ml of PTX-MOs-Gel, PTX-NCs-Gel or PTX-MCs-Gel was added in the bottom of the EP tube at 4 ℃ and incubated at 37 ℃. Then, 3.8 ml of pre-warmed PBS was carefully layered over the surface of the gel and shaken at 37 ℃, 100rpm. (A) At 0 and 14 d, the tubes were pictured by a digital camera. The phase interfaces were indicated by black arrows. (B) At various time points, 200 μl of medium was withdrawn along the PBS surface and replaced with an equal amount of PBS. The PTX concentration was determined by HPLC to calculate cumulative drug released. (C) A similar protocol to (A) was conducted to study *in vitro* erosion of DiR-MOs-Gel and DiR-NCs-Gel using DiR as fluorescence probe for molecular imaging.

3.5 In vivo erosion of the three hydrogels

Fig. 7 shows the *in vivo* erosion profiles of three hydrogel systems after being injected subcutaneously into ICR mouse models.

As seen in Fig. 7A, transparent or white gel formed instantly upon injection in all test groups. Three days later, white solid substance, likely the PTX precipitate, was obviously observed at the subcutaneous site of the mouse treated with PTX-MCs-Gel. However, neither gel nor precipitates were found at the injection site of the mice receiving PTX-MOs-Gel or PTX-NCs-Gel, consistent with previous literatures [14].

DiR-NCs-Gel and DiR-MOs-Gel were further studied for their differences in gel erosion *in vivo* (Fig. 7B). For DiR-MOs-Gel, fluorescence signal attenuated dramatically, probably with the erosion and disintegration of F127 gel. In contrast, fluorescence signal of DiR-NCs-Gel was still captured obviously although F127 gel had disappeared as demonstrated in Fig. 7A. These results were summarized in Fig. 7C. Therefore, DiR-NCs-Gel presented stronger drug retention effect than DiR-MOs-Gel.

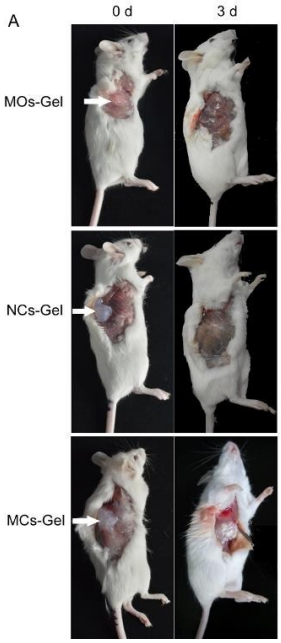

C

	0 d	3 d
MOs-Gel	Gel depot / **Payloads**	No gel /Little payloads
NCs-Gel	Gel depot / **Payloads**	No gel / Still much Payloads
MCs-Gel	Gel depot / **Payloads**	No gel / **Payloads-forming precipitation**

Fig. 7 *In vivo* erosion of the three hydrogel systems after being injected subcutaneously into ICR mouse models. (A) Gel formation and erosion observed by naked eye. The three arrows on the left side point to the formation of gel depots once injected, transparent for MOs-Gel, opacified for NCs-Gel and MCs-Gel. Three days later, nothing could be observed at the injection sites for both MOs-Gel and NCs-Gel while white materials precipitated from the MCs-Gel (arrow on the right side). (B) Payloads retention at local site after subcutaneous administration of NCs-Gel and MOs-Gel assayed by *in vivo* imaging. DiR was chosen as fluorescence probe (red area in the pictures). (C) Summary of *in vivo* erosion of the three hydrogel systems (red and blue font indicates DiR in vivo).

3.6 Intratumoral drug residue and distribution assay

Fig. 8A shows the intratumoral drug residual ratio of three hydrogels in 4T1 tumor. PTX-MCs-Gel exhibited the largest drug residual ratio, more than 30%, while PTX was

undetectable in DiR-MOs-Gel group at day 20 after administration. PTX-NCs-Gel presented a moderate drug residual ratio of about 13% at the same test time.

Fig. 8B displays the *ex vivo* fluorescence distribution of DiR-MOs-Gel and DiR-NCs-Gel at day 7 and day 16 after intratumoral injection. The whole tumor of DiR-NCs-Gel group showed significantly stronger fluorescence signal than that of DiR-MOs-Gel group at day 7 and day 16. No fluorescence inside of the tumor was detected for DiR-MOs-Gel at 16d.

To further determine distribution profiles of both DiR-MOs-Gel and DiR-NCs-Gel, the tumors were bisected and sliced. The imaging further illustrated the peritumoral and superficial distribution for DiR-MOs-Gel group but central distribution for the DiR-NCs-Gel group.

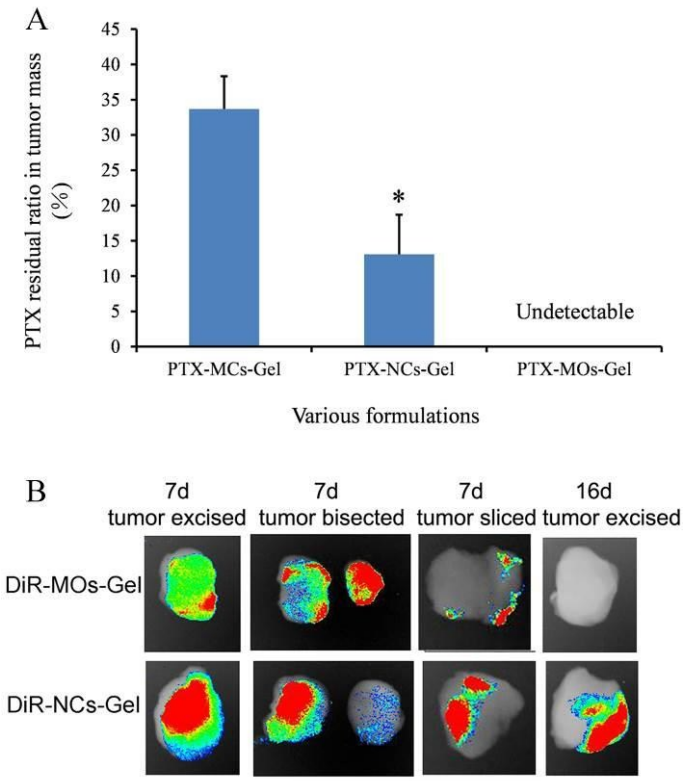

Fig. 8 Intratumoral drug residual amount assay and fluorescence distribution of the three hydrogel systems after being injected into 4T1 tumors on mice model. (A) Intratumoral residual amount of PTX at 20 days after i.t. injection of PTX-MCs-Gel, PTX-NCs-Gel and PTX-MOs-Gel (n=3/group). *p<0.05 vs PTX-MCs-Gel. (B) *Ex vivo* fluorescence images of excised (7 d tumor excised), bisected (7 d tumor bisected), and sliced (7d tumor sliced) xenograft tumors at 7 days after intratumoral administration as well as completely excised tumors at 16 days (16 d tumor excised).

3.7 Anti-tumor activity

The anti-tumor efficacy of different types of hydrogels was evaluated on 4T1 tumor-bearing BALB/c mice (Fig. 9). Each mouse received a single intratumoral injection of the each PTX hydrogel. As the result, PTX-NCs-Gel was significantly more effective than PTX-MOs-Gel and PTX-MCs-Gel against marine 4T1 in terms of tumor volume inhibition during a 20-day study (Fig. 9A). The PTX-MOs-Gel, however, showed the lowest anti-tumor efficacy under the same condition. The results of tumor weight assay were consistent with that of tumor volume determination (Fig. 9B).

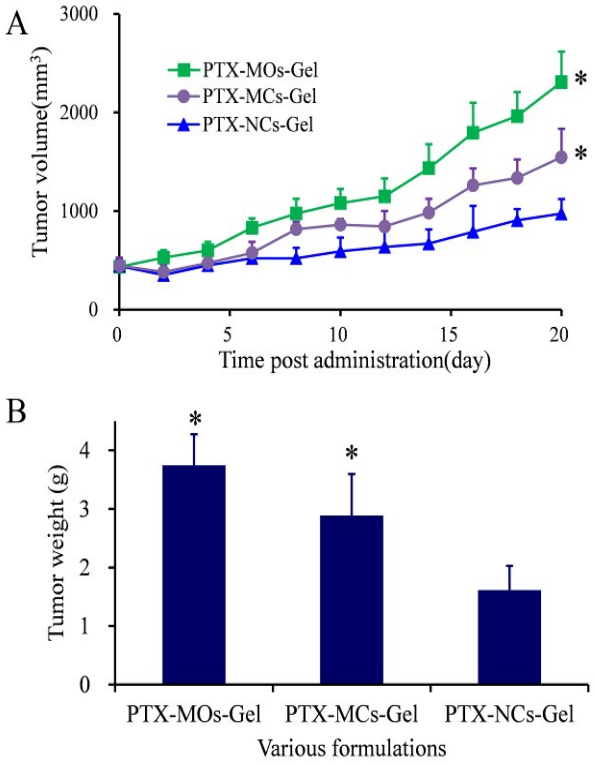

Fig. 9. *In vivo* anti-tumor activity against 4T1 tumor-bearing BALB/C mice after a single i.t. injection of PTX-MOs-Gel, PTX-NCs-Gel or PTX-MCs-Gel (n=6/group). (A) Tumor growth curve. (B) Tumor weight with various treatments.
* p<0.05 vs. PTX-NCs-Gel.

4. Discussion

It is expected that *in situ* thermo-sensitive hydrogel as a localized drug delivery system could provide high, long-term and continuous drug levels at the disease site to guarantee

satisfactory efficacy [11]. A great number of studies indicated that this goal could be reached to some extent by modifying thermo-sensitive polymers to enhance the function of hydrogel on drug loading and release [28-30]. However, little attention was paid to the impact of drug forms (e.g., drug state, morphology, particle size and so on) on the *in vitro* and *in vivo* performance of the whole hydrogel system. In this study, we conducted a comparative study of three kinds of F127 hydrogels with PTX in various forms (molecule, nanocrystal or microcrystal) to provide an insight into this effect and a basis for the design of thermo-sensitive hydrogel.

We firstly prepared the three hydrogels using hydrophobic payloads, PTX or DiR. The preparation of MOs-Gel was reached by addition of PTX/DiR solution into hydrogel as well as addition of Tween-80 into F127 as solubilizer [25]. PTX-MCs-Gel was formulated by dispersing high levels of PTX powders into hydrogel directly. But unfortunately, DiR-MCs-Gel showed little fluorescence due to fluorescence quenching of micron-size DiR [27]. So, in some of the tests, as in Fig. 6C and Fig. 7B, we could not use DiR-MCs-Gel for the related comparison. As for preparation of NCs-Gel, micron-grade crude PTX powders must be firstly processed into nano-sized crystals before dispersion into the gel following our previous method [21].

We then assayed the states of drug dispersed in the three hydrogel systems qualitatively and quantitatively. As shown in Fig. 4, the particle size of MCs-Gel determined by DLS seems to be less than 1 μm, discrepant with TEM results, likely due to inaccuracy of DLS determination for the large micro-sized particles. We believe that the particle size of PTX-MCs were up to more than 2 μm from the results of TEM and microscope (Fig. 3). According to our research design (Fig. 1), drug forms in these three hydrogels represent three dimensions which may affect the performances of hydrogel on drug loading and release, further leading to the differences on efficacy. Besides of the qualitative assay by TEM and DLS, a quantitative assay on their compositions further confirmed that molecules,

nanocrystals or microcrystals are the dominant drug form in the corresponding gels. The determination of free drug also indicated that drug would not transport between hydrophobic domains and hydrophilic domains of hydrogel for the three hydrogels.

Drug loading is the premise for sustained-release hydrogel to exert its efficacy. High drug loading amount is necessitated for thermo-sensitive hydrogel to maintain a long-term, high drug level at local site. Obviously, drug particles were easier to achieve high drug loading than the drug molecules incorporated into F127 micelles by hydrophobic interaction [31]. Expectedly, F127 gel could load 3 mg/ml of PTX-NCs or PTX-MCs, far higher than other F127 hydrogel systems reported previously [21]. Moreover, the states of PTX dispersed in hydrogel were quite different, almost 100% of free drug in MOs-Gel but less than 5% in NCs-Gel or MCs-Gel, which would probably be related to their significant differences in curative effect (Table. 1) [32-34].

The different drug states and size may result in obviously different physical stability of hydrogels. At the same drug levels, PTX-NCs-Gel was distinctly superior to PTX-MCs-Gel in terms of drug-dispersion uniformity, storage stability as well as stable drug release (Fig. 5 and Fig. 6). Because both PTX-NCs and PTX-MCs were rod-shape, the divergence of stability mainly resulted from their different particle size, leading to different dispersion even sedimentation in gel. In addition, due to the high viscosity of F127 in gel state, the stability of PTX-NCs-Gel is obviously better than nanocrystal solution which is usually regarded as an instable system in water medium [35]. However, such viscous dispersion medium could not prevent the larger microcrystals from settling down. It is worth pointing out that although the instability of hydrogel can be resolved partly by shacking before use, it may lead to inaccuracy in dosing and inconvenience in clinic use. Therefore, introduction of nanocrystals into hydrogel may be an appropriate option in the aspect of stability.

It has been widely reported that drug release from F127 hydrogel is based on gel erosion

mechanism for hydrophobic drugs [12]. In in vitro gel erosion experiments, F127 micelles shed from MOs-Gel into the PBS medium, evidenced by the high percentage of cumulative drug released and the erosion of DiR-MOs-Gel (Fig. 6). Additionally, the differences in gel erosion and drug release among the three hydrogels were significant (Fig. 6A and B). Rapid gel erosion of PTX-MOs-Gel led to fast PTX release, consistent with previous studies on F127 gel. Like MOs-Gel, MCs-Gel also disintegrated totally at the end of experiment. This is probably because the rapid precipitation of PTX microcrystals separated drug and hydrogel, leading to little interaction between drug microcrystals and gel. Such rapid gel erosion and drug precipitation caused low cumulative percentage of PTX released, which may limit its curative effect in vivo. Interestingly, NCs-Gel could preserve gel-like structure during the whole process of gel erosion, probably due to the interaction between rod-shape nanocrystals and F127 gel which needs further investigation in the future (Fig. 6A). The above differences in gel erosion and drug release among the three hydrogels could be attributed to the drug states and their particle size. Taken together, on one hand, long rod-like microcrystals suspended in the gel seem to be too large to maintain stable drug release. On the other hand, after diluted by PBS or body fluid, 20-nm spherical micelles shedding from the F127 gel appear to be too small to remain MOs-Gel at the local site. So the PTX-NCs with intermediate particle size may be the optimal forms for F127 gel to keep stable gel erosion and prolonged drug release.

As shown in Fig. 7, the *in vivo* erosion was only performed for three days because we had already observed significant differences among the three hydrogels, consistent with *in vitro* erosion and the characteristics of F127 reported by literature [13, 14]. In Fig. 7A, it seems that no gel retention was observed for NCs-Gel, which contradicts with the results of gel erosion in vitro (Fig. 6A). When the gels were injected subcutaneously, it is easy for them to be spread out under the derma friction and so difficult to preserve loosening gel structure for three days in vivo. Although DiR-NCs-Gel and DiR-MOs-Gel did not show visible differences in gel retention, as a matter of fact, the differences in fluorescence retention are

striking as in Fig. 7B.

As shown in Fig.8, the highest drug residual ratio in the tumor was found in PTX-MCs-Gel, but it could not ensure stable drug release , evidenced by the white drug precipitate observed at the injection site (Fig. 8A), which may attenuate the antitumor efficacy greatly. Furthermore, the data of PTX residual in tumor for the three hydrogels were consistent with the results of gel erosion and the drug release *in vitro* and *in vivo* (Fig. 6, Fig.7). Finally, the feature of fluorescence distribution of DiR-MOs-Gel and DiR-NCs-Gel was in accordance with the gel erosion characteristics and intra-tumoral drug residual assay (Fig. 7B and Fig.8).

As expected from the above studies, PTX-NCs-Gel was the most effective among the three hydrogel systems in enhancing anti-tumor efficacy against 4T1 tumors (Fig. 9). The limitations of PTX-MOs-Gel and PTX-MCs-Gel on anti-tumor activity could attribute to different reasons. Poor efficacy of PTX-MOs-Gel was due to rapid gel erosion and drug release, while the effect of PTX-MCs-Gel was limited by the instable and little drug release during the process of gel erosion. Therefore, PTX-NCs-Gel presented the strongest anti-tumor efficacy, mainly due to the introduction of NCs which possesses moderate particle size and rod-shape structure, providing gel with good performance on drug loading and drug release.

5. Conclusion

In this study, we performed a comparative study of thermo-sensitive F127 hydrogels with water-insoluble PTX in different scale and dispersion states: micelles incorporating MOs (20 nm), NCs (120 nm) or MCs (>2 μm). On one hand, MCs facilitate the gel to achieve high drug loading, but hardly to release drug, limiting its anti-tumor efficacy. On the other hand, MOs-Gel could release drug too quickly to maintain drug at the injection site, leading to poor curative effect. The comparative study showed that NCs-Gel presented an optimal performance by high drug loading associated with moderate drug release rate, resulting from

the form of nanocrystals in gel (rod-shape with intermediate particle size). Such superior function of NCs-Gel further led to its preferable anti-tumor efficacy. This study provides a new basis for the future design of thermo-sensitive hydrogel for locally delivering hydrophobic anti-cancer agents.

Acknowledgments

This study was supported by the National Natural Science Foundation of China (no. 81130059), the National Basic Research Program of China (973 program, 2015CB932100), the Key Project from the Ministry of Science and Technology (2014ZX09507-001-10), and Innovation Team of Ministry of Education (no. BMU20110263).

References

1. Y. H. Bae and K. Park, *J Control Release*, 2011, **153**, 198-205.
2. J. B. Wolinsky, Y. L. Colson and M. W. Grinstaff, *J Control Release*, 2012, **159**, 14-26.
3. K. Park, *J Control Release*, 2013, **172**, 391.
4. C. Wang, C. Long, C. Xie, X. Chen, L. Zhang, B. Chu, Y. Wang, F. Luo and Z. Qian, *J Biomed Nanotechnol*, 2013, **9**, 357-366.
5. S. S. Chakravarthi, De S, D. W. Miller and D. H. Robinson, *Int J Pharm*, 2010, **383**, 37-44.
6. R. Liu, J. B. Wolinsky, P. J. Catalano, L. R. Chirieac, A. J. Wagner, M. W. Grinstaff, Y. L. Colson and C. P. Raut, *Ann Surg Oncol*, 2012, **19**, 199-206.
7. A. P. Griset, J. Walpole, R. Liu, A. Gaffey, Y. L. Colson and M. W. Grinstaff, *J Am Chem Soc*, 2009, **131**, 2469-2471.
8. F. Qian, A. Szymanski and J. Gao, *J Biomed Mater Res*, 2001, **55**, 512-522.
9. E. Ruel-Gariepy, M. Shive, A. Bichara, M. Berrada, D. Le Garrec, A. Chenite and J. C. Leroux, *Eur J Pharm Biopharm*, 2004, **57**, 53-63.
10. H. Brem, S. Piantadosi, P. C. Burger, M. Walker, R. Selker, N. A. Vick, K. Black, M. Sisti, S. Brem, G. Mohr and A. Et, *Lancet*, 1995, **345**, 1008-1012.
11. N. L. Elstad and K. D. Fowers, *Adv Drug Deliv Rev*, 2009, **61**, 785-794.
12. G. Dumortier, J. L. Grossiord, F. Agnely and J. C. Chaumeil, *Pharm Res*, 2006, **23**, 2709-2728.
13. B. Jeong, Y. H. Bae, D. S. Lee and S. W. Kim, *Nature*, 1997, **388**, 860-862.
14. D. Cohn, G. Lando, A. Sosnik, S. Garty and A. Levi, *Biomaterials*, 2006, **27**, 1718-1727.
15. J. Xu, X. Li, F. Sun and P. Cao, *J Biomater Sci Polym Ed*, 2010, **21**, 1023-1038.
16. G. Bajaj, M. R. Kim, S. I. Mohammed and Y. Yeo, *J Control Release*, 2012, **158**, 386-392.
17. S. Nie, W. L. Hsiao, W. Pan and Z. Yang, *Int J Nanomedicine*, 2011, **6**, 151-166.

18. X. Guo, F. Cui, Y. Xing, Q. Mei and Z. Zhang, *Pharmazie*, 2011, **66**, 948-952.
19. R. V. Contri, T. Katzer, A. F. Ourique, S. A. Da, R. C. Beck, A. R. Pohlmann and S. S. Guterres, *J Biomed Nanotechnol*, 2014, **10**, 820-830.
20. Z. P. Chen, W. Liu, D. Liu, Y. Y. Xiao, H. X. Chen, J. Chen, W. Li, H. Cai, W. Li, B. C. Cai and J. Pan, *J Control Release*, 2012, **162**, 628-635.
21. Z. Lin, W. Gao, H. Hu, K. Ma, B. He, W. Dai, X. Wang, J. Wang, X. Zhang and Q. Zhang, *J Control Release*, 2014, **174**, 161-170.
22. X. Lu, F. Zhang, L. Qin, F. Xiao and W. Liang, *Drug Deliv*, 2010, **17**, 255-262.
23. F. Liu, J. Y. Park, Y. Zhang, C. Conwell, Y. Liu, S. R. Bathula and L. Huang, *J Pharm Sci*, 2010, **99**, 3542-3551.
24. J. E. Matthew, Y. L. Nazario, S. C. Roberts and S. R. Bhatia, *Biomaterials*, 2002, **23**, 4615-4619.
25. Y. Yang, J. Wang, X. Zhang, W. Lu and Q. Zhang, *J Control Release*, 2009, **135**, 175-182.
26. C. Mamot, D. C. Drummond, C. O. Noble, V. Kallab, Z. Guo, K. Hong, D. B. Kirpotin and J. W. Park, *Cancer Res*, 2005, **65**, 11631-11638.
27. H. Cho, G. L. Indig, J. Weichert, H. C. Shin and G. S. Kwon, *Nanomedicine*, 2012, **8**, 228-236.
28. A. Sosnik and D. Cohn, *Biomaterials*, 2005, **26**, 349-357.
29. G. G. Niu, A. B. Djaoui and D. Cohn, *Polymer*, 2011, **52**, 2524-2530.
30. D. M. Henn, R. A. Wright, J. W. Woodcock, B. Hu and B. Zhao, *Langmuir*, 2014, **30**, 2541-2550.
31. B. E. Rabinow, *Nat Rev Drug Discov*, 2004, **3**, 785-796.
32. R. Shegokar and R. H. Muller, *Int J Pharm*, 2010, **399**, 129-139.
33. L. Gao, G. Liu, J. Ma, X. Wang, L. Zhou and X. Li, *J Control Release*, 2012, **160**, 418-430.
34. J. Shi-Ying, H. Jin, J. Shi-Xiao, L. Qing-Yuan, B. Jin-Xia, H. G. Chen, L. Rui-Sheng, W. Wei and Y. Hai-Long, *Chin J Nat Med*, 2014, **12**, 71-80.

35. L. Wu, J. Zhang and W. Watanabe, *Adv Drug Deliv Rev*, 2011, **63**, 456-469.